# LATTICE BOLTZMANN SIMULATION OF FLOW OVER A CIRCULAR CYLINDER AT MODERATE REYNOLDS NUMBERS

by

***Dharmaraj ARUMUGA PERUMAL[a*], Gundavarapu V. S. KUMAR[b], and Anoop K. DASS[b]***

[a]Automotive Research Centre, SMBS, VIT University, Vellore, Tamilnadu, India,
[b] Department of Mechanical Engineering, Indian Institute of Technology Guwahati, Guwahati, India

Original scientific paper
DOI: 10.2298/TSCI110908093A

*This work is concerned with Lattice Boltzmann computation of 2-D incompressible viscous flow past a circular cylinder confined in a channel. Computations are carried out both for steady and unsteady flows and the critical Reynolds number at which symmetry breaks and unsteadiness sets in is predicted. Effects of Reynolds number, blockage ratio and channel length are studied in some details. All the results compare quite well with those computed with continuum-based methods, demonstrating the ability and usefulness of the Lattice Boltzmann method in capturing the flow features of this interesting and fluid-mechanically rich problem.*

Key words: *2-D, circular cylinder, confined channel, Lattice Boltzmann method, D2Q9 model*

## Introduction

The classical problem of viscous incompressible flow over a circular cylinder confined in a channel is one of the most widely studied problems in computational fluid dynamics (CFD) [1]. This flow, at lower Reynolds numbers (Re), is steady whereas at higher Reynolds numbers unsteadiness develops and the flow becomes periodic. The periodic flow is characterized by the so called von Karman vortex street generated by alternate and periodic shedding of vortices from the top and bottom. This type of flow problems frequently arise in various engineering fields which offer tough challenges particularly at high Reynolds numbers [2]. Because of its popularity, a plethora of numerical, theoretical and experimental results are available for this problem in the literature [3-10].

Some of the notable works on flow past a circular cylinder by the conventional numerical methods include those of Fornberg [4], Braza [5] and Franke *et al*., [6]. Calhoun [7] described a finite-difference/finite-volume algorithm for solving the streamfunction-vorticity equations in an irregular geometry such as flow past a circular cylinder. Sahin and Owens [8] used a finite volume method to solve the flow field around a circular cylinder confined in a channel. They investigated lateral wall proximity effects on stability, Strouhal number, hydrodynamic forces and wake structure behind the cylinder for a wide range of blockage ratios. Zovatto and Pedrizzetti [9] presented solutions for the flow past a circular cylinder placed inside a plane channel at various distances

* Corresponding author; e-mail: perumal.d@vit.ac.in

from the walls for different Reynolds number from steady flows to the initiation of the vortex shedding regime. Anagnostopoulos and Iliadis [10] used the finite element technique for the solution of steady and unsteady flow around a circular cylinder at Re = $10^6$ for different blockage ratios. More recently, Singha and Sinhamahapatra [11] studied the flow over a confined cylinder problem and confirmed that transition to vortex shedding regime is delayed when the channel walls are close to the cylinder because of the interaction between the vortices from the channel wall and cylinder wake.

In the last two decades lattice Boltzmann method (LBM), a non-conventional numerical method for applications in CFD has gained popularity [12]. Distinguished from conventional simulation methods like finite difference method (FDM), finite volume method (FVM), and finite element method (FEM), the lattice Boltzmann method provides stable and efficient numerical calculations for the macroscopic behaviour of fluids, although describing the fluid in a microscopic way [13-21]. It is observed that a large number of attempts have been made to study flow over a cylinder using continuum-based methods [22-25] and a very few attempts have been made using lattice Boltzmann method. This paper aims at bringing out the merits of the lattice Boltzmann method in capturing various flow features of this interesting and fluid-mechanically rich problem. Besides presenting steady and unsteady results for various Reynolds numbers, the present work also predicts, through LBM, the critical Reynolds number at which unsteadiness sets in.

## Lattice Boltzmann method

In the last one and a half decade or so LBM has emerged as a new and effective approach of computational fluid dynamics (CFD) and it has achieved considerable success in simulating fluid flows and heat transfer [14]. The justification for this approach is the fact that the collective behaviour of many microscopic particles is behind the macroscopic dynamics of a fluid and this dynamics is not particularly dependent on the details of the microscopic phenomena exhibited by the individual molecules. The LBM therefore uses a simplified kinetic model to work with. In spite of its kinetic origin LBM however, is mainly used to capture the macroscopic behaviour represented by variables describing fluid flow and heat transfer. The LBGK model with the single time relaxation, which is a commonly used lattice Boltzmann method, is given by [15]:

$$f_i(\vec{\mathrm{x}} + \vec{\mathrm{e}}_i \Delta t, t + \Delta t) - f_i(\vec{\mathrm{x}}, t) = -\frac{1}{\tau}[f_i(\vec{\mathrm{x}}, t) - f_i^{eq}(\vec{\mathrm{x}}, t)] \tag{1}$$

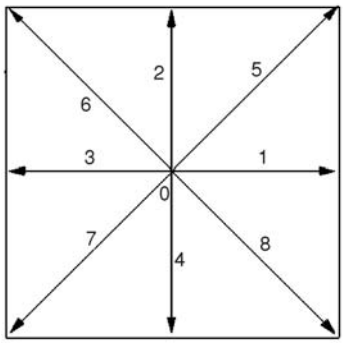


**Figure 1. 2-D nine-velocity square lattice model**

where $f_\mathrm{i}$ is the particle distribution function, $f_i^{eq}(\vec{\mathrm{x}}, t)$ – the equilibrium distribution function at $\vec{\mathrm{x}}$, $t$, $\vec{\mathrm{e}}_i$ – the particle velocity along the $i^{\mathrm{th}}$ direction, and $\tau$ – the time relaxation parameter. The D2Q9 square lattice (fig. 1) used here has nine discrete velocities. The particle velocities are defined as [15]:

$$\begin{aligned} e_i &= 0, 0, \quad i = 0 \\ e_i &= \cos\left[\frac{\pi}{4}(i-1)\right], \sin\left[\frac{\pi}{4}(i-1)\right], \quad i = 1,\ 2,\ 3,\ 4 \\ e_i &= \sqrt{2}\left[\frac{\pi}{4}(i-1)\right], \sin\left[\frac{\pi}{4}(i-1)\right], \quad i = 5,\ 6,\ 7,\ 8 \end{aligned} \tag{2}$$

The macroscopic quantities such as density $\rho$ and momentum density $\rho\vec{u}$ are defined as velocity moments of the distribution function $f_i$ as follows:

$$\rho = \sum_{i=0}^{N} f_i \tag{3}$$

$$\rho u = \sum_{i=0}^{N} f_i e_i \tag{4}$$

where $N = 8$. The density is determined from the particle distribution function. The density and the velocities satisfy the Navier-Stokes equations in the low-Mach number limit [12].

In the D2Q9 square lattice, a suitable equilibrium distribution function that has been proposed is [15]:

$$\begin{aligned} f_i^{eq} &= \rho w_i \left[1 - \frac{3}{2}\vec{u}^2\right], \quad i = 0 \\ f_i^{eq} &= \rho w_i [1 + 3(\vec{e}_i \vec{u}) + 4.5(\vec{e}_i \vec{u})^2 - 1.5\vec{u}^2], \quad i = 1, 2, 3, 4 \\ f_i^{eq} &= \rho w_i [1 + 3(\vec{e}_i \vec{u}) + 4.5(\vec{e}_i \vec{u})^2 - 1.5\vec{u}^2], \quad i = 5, 6, 7, 8 \end{aligned} \tag{5}$$

where the lattice weights are given by $w_0 = 4/9$, $w_1 = w_2 = w_3 = w_4 = 1/9$, $w_5 = w_6 = w_7 = w_8 = 1/36$.

The relaxation time which fixes the rate of approach to equilibrium is related to the viscosity by [13]:

$$\tau = \frac{6\nu + 1}{2} \tag{6}$$

where $\nu$ is the kinematic viscosity measured in lattice units.

## Problem and associated features of LBM

The schematic diagram of the flow past a circular cylinder confined in a channel is shown in fig. 2. The present problem deals with a cylinder with circular cross-section with diameter $D$ mounted centrally inside a plane channel of height $H$ with blockage ratio $B = H/D$. The channel length $L$ is fixed at $L/D = 50$ to reduce the influence of outflow boundary conditions on accuracy. An upstream length of $l = L/4$ or $12.5D$ has been chosen. In this problem, the inlet boundary conditions are given by a uniform velocity profile. The LBM simulation studies are carried out for different values of Reynolds numbers $\mathrm{Re} = UD/\gamma$, where $U$ is the velocity at the channel entry and $D$ is the cylinder diameter.

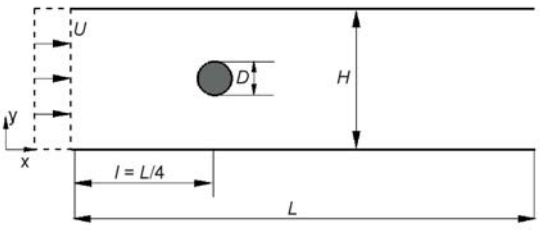


**Figure 2. Schematic diagram of the flow past a circular cylinder confined in a channel**

It is known that, in LBM simulation the boundary condition for the particle distribution function on a solid wall can be given by a popular approach known as bounce-back scheme [13]. Therefore, in the present work, we use bounce-back boundary condition on the top and bottom walls, which indicates no-slip. We use bounce-back with additional momentum to the inlet boundary with known velocity to provide the required inlet condition for the particle distribution function $f_i$, as proposed by Yu *et al*. [14]. It creates a mechanism for the pressure wave from

the interior of the computational domain to interact with the inlet boundary and it can be reflected back. At the outlet of the computational domain, fi can usually be approximated by a simple extrapolation boundary condition proposed by Guo *et al.* [21]. On the solid curved boundary, *i. e*., on the surface of the cylinder, a robust second order accurate boundary treatment proposed by Bouzidi *et al*. [16] is used for the particle distribution function.

In the present LBM simulation, we use the momentum exchange method to compute the fluid force on the circular cylinder. The total force acting on a solid body by fluid can be written as [14]:

$$F = \sum_{all x_b} \sum_{\alpha=1}^{N_d} e_{\bar{\alpha}} [\tilde{f}_\alpha (x_\mathrm{b}, t) + \tilde{f}_\alpha (x_\mathrm{b} + e_{\bar{\alpha}} \delta t, t)][1 - w(x_\mathrm{b} + e_{\bar{\alpha}})] \frac{\delta x}{\delta t} \tag{7}$$

where $N_\mathrm{d}$ is the number of non-zero lattice velocity vectors and $w(x_\mathrm{b} + e_{\bar{\alpha}})$ is an indicator, which is 0 at $x_\mathrm{f}$ and 1 at $x_\mathrm{b}$. The inner summation calculates the momentum exchange between a solid node at $x_b$, and all possible neighbouring fluid nodes around that solid node. The outer summation calculates the force contributed by all boundary nodes $x_\mathrm{b}$. The two most important characteristic quantities of flow around a cylinder are the coefficient of drag and coefficient of lift. The coefficients are defined as:

– coefficient of drag

$$C_\mathrm{D} = \frac{F_\mathrm{x}}{\frac{1}{2}\rho A U_\alpha^2}$$

– coefficient of lift

$$C_\mathrm{L} = \frac{F_\mathrm{y}}{\frac{1}{2}\rho A U_\alpha^2}$$

where $F_\mathrm{x}$ and $F_\mathrm{y}$ are the x- and y-components of the total fluid force acting on the cylinder, $A$ – the projected area. Themes of present studies are:

– for a fixed blockage ratio to study the circular cylinder flow field characteristics,
– for different blockage ratios to study the circular cylinder flow field characteristics.
– for different outlet boundary locations to study the cylinder flow field characteristics, and
– for different lengthwise cylinder locations to study the flow field characteristics.

## Results and discussions

### *Fixed blockage ratio*

For a blockage ratio $B = H/D = 8$ computations are carried out at different Reynolds numbers with the help of lattice Boltzmann method with single-relaxation-time collision model. The lattice size of 500 × 80 is used for the present configuration.

– *Steady flow*

Streamline patterns for a blockage ratio B = 8 at Reynolds numbers Re = 4, 5, 10, 20, 30, and 40 are shown in fig. 3. At low Reynolds number (Re = 4) the steady flow past the circular cylinder persists without separation as shown in fig. 3(a). As Reynolds number increases the separation of the steady flow laminar boundary layer is clearly observed in figs. 3(b) and 3(c). At Re = 5, separation of steady flow just begins and as Reynolds number increases a pair of vortices develops behind the circular cylinder and they grow in size with Reynolds number. It is seen, figs. 3(c)-3(f), that two vortices downstream of the cylinder, symmetrically placed about the

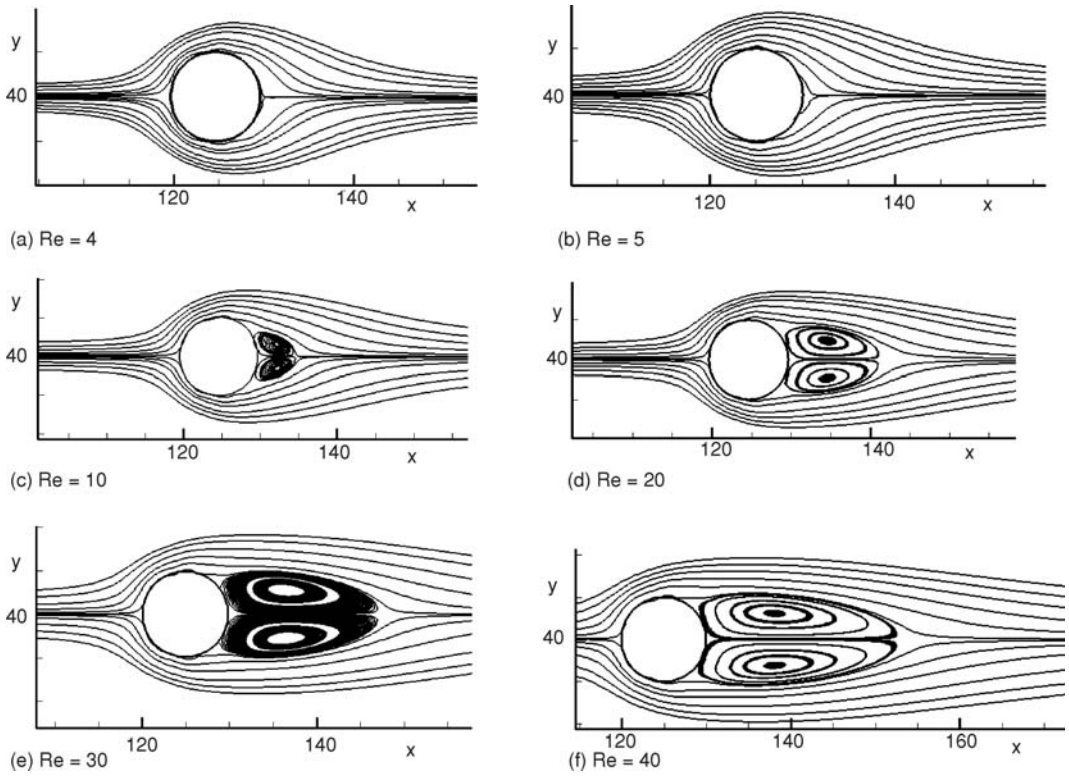


**Figure 3. Streamline patterns for steady flows past a circular cylinder at different Reynolds numbers for a blockage ratio $B = 8$: (a) Re = 4, (b) Re = 5, (c) Re = 10, (d) Re = 20, (e) Re = 30, and (f) Re = 40; lattice size: 500 × 80**

channel centreline, develop and remain attached to the cylinder. From figs. 3(a)-3(f), it is again seen that for steady flows the size of the vortices increases with Reynolds number. In tab. 1, we present the coefficient of drag for different steady-flow Reynolds numbers. Expectedly as the Reynolds number increases coefficient of drag (CD) decreases.

**Table 1. Coefficient of drag for different steady-flow Reynolds numbers**

| Authors | Re = 10 | Re = 20 | Re = 30 | Re = 40 |
|---|---|---|---|---|
| Tritton (experimental) [2] | – | 2.22 | – | 1.48 |
| Fornberg (numerical) [4] | – | 2.00 | – | 1.50 |
| Calhoun (numerical) [7] | – | 2.19 | – | 1.62 |
| Present LBM | 3.21 | 2.25 | 1.74 | 1.50 |

– *Unsteady flow*

In our LBM simulation the periodic flow is computed at Re = 60, 100 and 150 for which the streamline patterns at a certain instant are shown in figs. 4(a)-(c). At Re = 60, many experimental and numerical results have shown conclusively that eventually asymmetry sets in

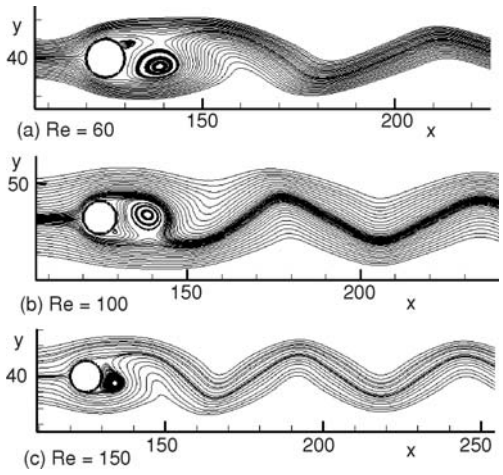


**Figure 4. Instantaneous streamline line patterns for flows past a circular cylinder at different Reynolds numbers for a blockage ratio $B$ = 8: (a) Re = 60 (b) Re = 100, and (c) Re = 150; lattice size: 500 × 80**

and the flow becomes unsteady. From figs. 4(a)-(c), it is seen that as the Reynolds number increases the streamline patterns becomes wavy and sinuous on the rear-side of the circular cylinder. Figure 5 depicts the vorticity contours for flow past a circular cylinder at various Reynolds numbers (Re = 4, 5, 40, 60, 100, and 150). Interestingly for the steady flow, on the line of symmetry downstream of the cylinder flow is irrotational. Steady flow vortices seem to be more and more elongated as the Reynolds number increases. From the vorticity contours we clearly observe that vortices with negative and positive vorticies are alternatively shed at Re = 60, 100, and 150. This is known as the famous von Karman vortex street. The point of separation is also clearly observed from the vorticity contours. From figs. 5(d)-(f) it is seen that for a fixed length of the confining channel, number of periodic vorticities shed increases with Reynolds number. Thus without quantifying the associated frequencies for the Reynolds numbers, it is possible to say that frequency of vortex shedding increases as Reynolds number increases.

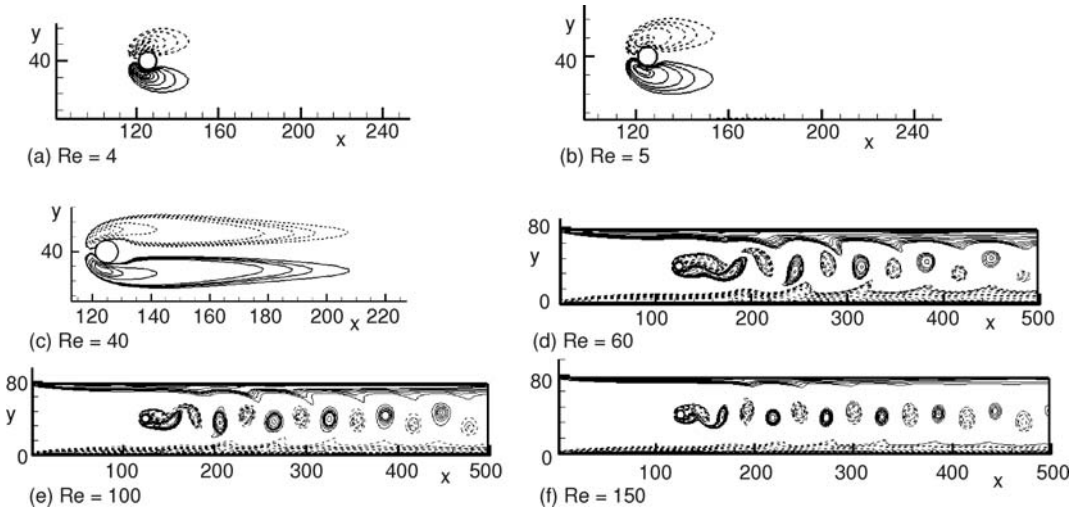


**Figure 5. Vorticity contours for flows past a circular cylinder at different Reynolds numbers for a blockage ratio B = 8: (a) Re = 4, (b) Re = 5, (c) Re = 40, (d) Re = 60, (e) Re = 100, and (f) Re = 150; lattice size: 500 × 80**

In order to study the flow field characteristics, velocity variation along the channel centreline are presented for Re = 45. Figure 6 shows the distributions of x- and y-velocity com-

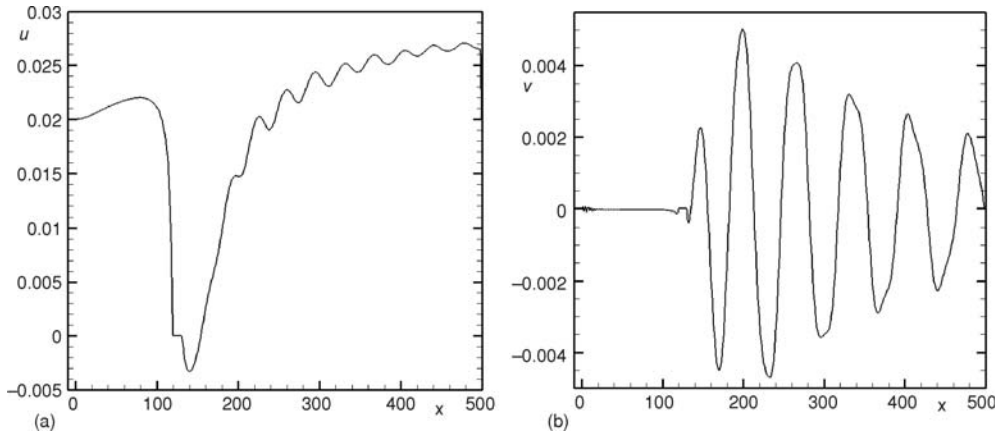


**Figure 6. Instantaneous results at a certain moment for the flow over a circular cylinder: (a) stream wise *u*, and (b) cross stream, *v*, velocities along the centerline (*y* = 0); Re = 45, lattice size: 500×80**

ponents along the channel centreline. It is observed that fluctuations of velocity at the exit boundary are small. At the surface of the cylinder velocity is zero and at upstream locations flow velocity varies smoothly without much oscillation. Figure 7 shows similar plots when the channel length is increased from 500 to 600 lattice units. It is observed that the fluctuation at the outflow boundary is smaller for this increased channel length. This is the justification for applying the outflow boundary condition at a large distance from the cylinder.

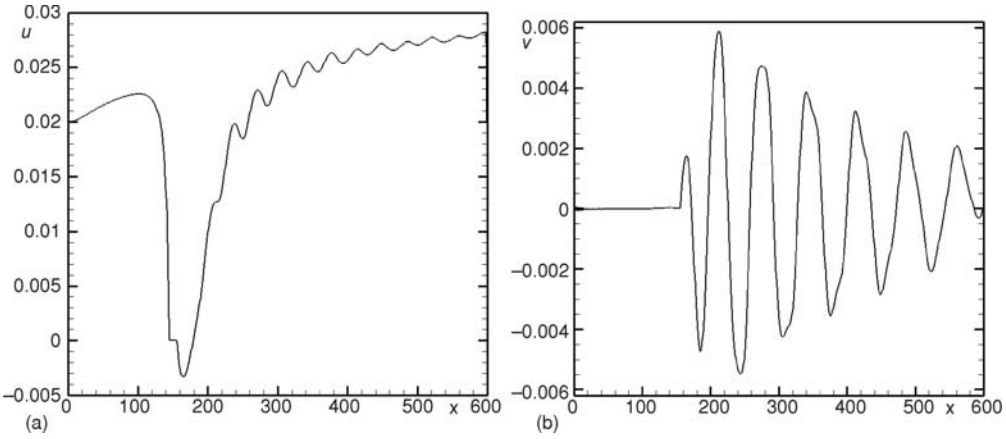


**Figure 7. Instantaneous results at a certain moment for the flow over a circular cylinder: (a) stream wise *u*, and (b) cross stream *v*, velocities along the centerline (*y* = 0); Re = 45, lattice size: 600 × 80**

Figure 8 shows the periodic time variation of the lift coefficient ($C_L$) and drag coefficient ($C_D$) for the flow past a circular cylinder at Re = 60 and 100. It is seen that for each time period, $C_D$ has two crests and two troughs of unequal amplitudes, which are a consequence of the periodic vortex shedding from the top and bottom surfaces. The same figure shows that $C_L$ for each time period has just one trough and one crest; this is because $C_L$ is not influenced by the

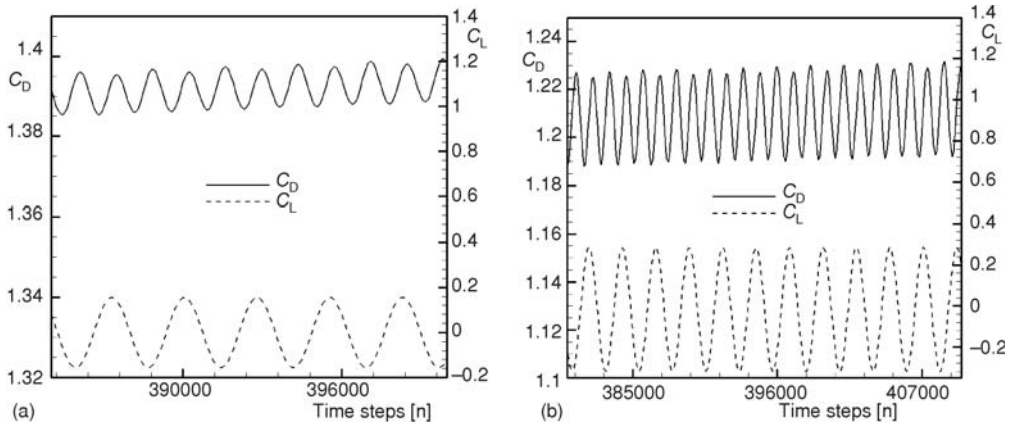


**Figure 8. Flow over a circular cylinder: Time dependent lift and drag coefficients ($C_L$ and $C_D$) at (a) Re = 60 and (b) Re = 100 on a lattice size of 500 × 80**

**Table 2. Mean drag coefficient and coefficient of lift for the flow over a cylinder at Re = 100**

| Authors | $C_{Dmean}$ | $C_L$ |
|---|---|---|
| Braza *et al.* [5] | 1.364 | ±0.25 |
| Calhoun [7] | 1.330 | ±0.298 |
| Present LBM | 1.290 | ±0.289 |

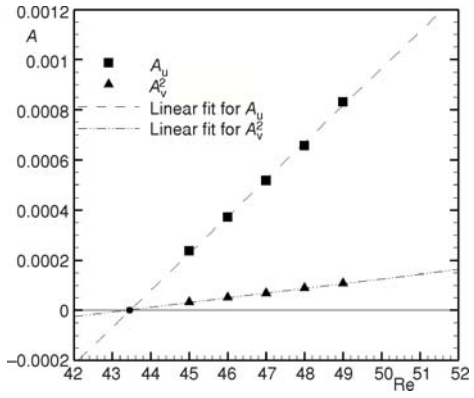


**Figure 9. Onset of unsteadiness for a blockage ratio $B$ = 8.0 ($A$ for $u$, $A^2$ for $v$ as a function of Re)**

pressure distribution on the rear side of the cylinder, which is strongly influenced by the vortex shedding at the top and bottom sides of the cylinder. The value of the lift force fluctuation is directly connected to the formation and shedding of the eddy and, therefore, its value varies between a positive maximum and a negative maximum of equal magnitude. In tab. 2, we present the mean drag coefficient and coefficient of lift for Re = 100. All the results computed with present LBM compare well with existing numerical results [17-19].

Figure 9 shows how a critical Reynolds number can be roughly predicted [20]. Here Au indicates, at a point in the wake region, the amplitude of fluctuations of u when periodicity sets in and Av indicates the same for $v$. For five different Reynolds numbers, close to the critical, $A_u$ and $A_u^2$ are plotted against Re. Linear fits through these points intersects at a point, which approximately indicates the Reynolds number at which vortex shedding starts. Here it is observed that for a blockage ratio $B$ = 8 critical Reynolds number is between 43 and 44.

### *Different blockage ratios*

To study the effect of different blockage ratios Re = 44 is chosen in the present work. Cylinder location of $l = L/4$ and a channel length of $L/D = 50$ is considered here. Figure10 shows the vorticity contours for confined flow over a circular cylinder at different blockage ratios. Six different blockage ratios $B$ = 4, 7, 8, 10, 15, 20, 30 and 40 are studied in the present work. From

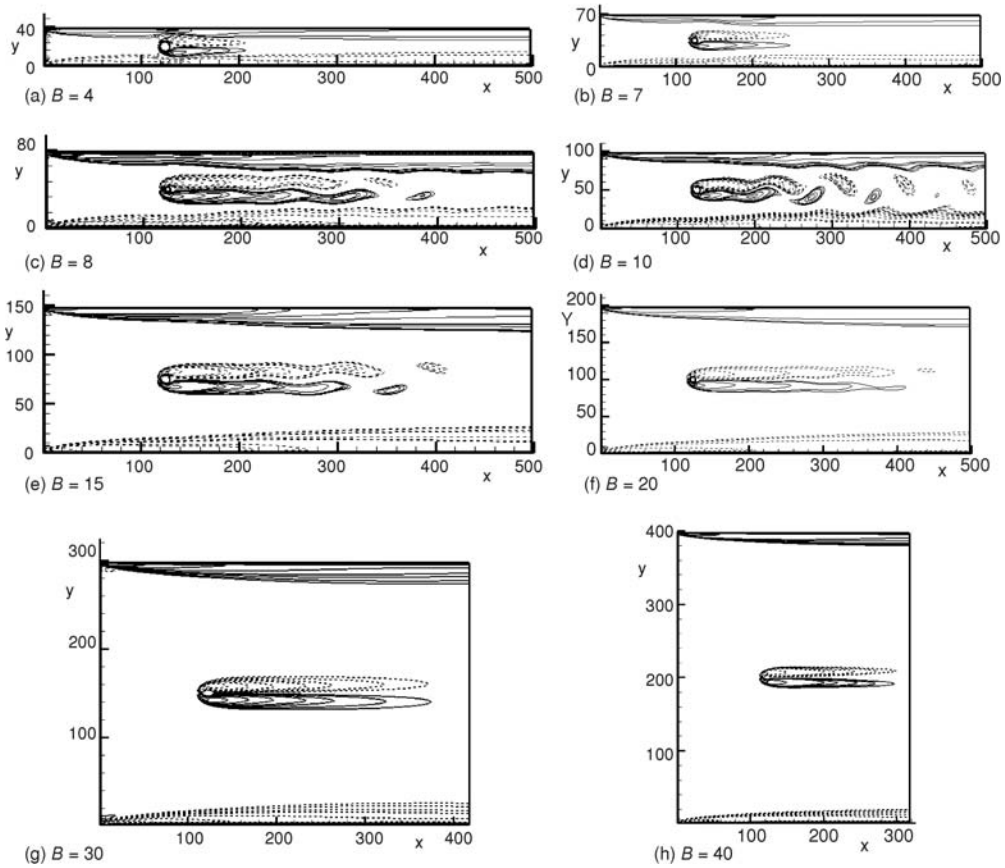


**Figure 10. Instantaneous vorticity contours for flows past a circular cylinder at different blockage ratios (a) $B = 4$, (b) $B = 7$, (c) $B = 8$, (d) $B = 10$, (e) $B = 15$, (f) $B = 20$, (g) $B = 30$, and (h) $B = 40$**

our LBM simulations we observe that the moderate blockage ratio $B = 8$ onwards unsteadiness develops in the flow field. The flow happens to be steady for lower values of blockage ratio $B$ (4 and 7 here). It can be clearly observed that at low blockage ratios wall boundary layer has strong influence over the flow around the cylinder so that it inhibits vortex shedding. Flow becomes unsteady at higher values of blockage ratio $B$. As the blockage ratio increases computation time required for obtaining unsteadiness increases.

### *Different outlet boundary conditions*

To study the effect of different outlet boundary locations Re = 44 is taken. In this case, blockage ratio $B = 8$ and upstream length $l = L/4$ is chosen. In the present case $L/D = 30$, 40, 50, and 60 are considered. Figure 11 shows the vorticity contours for confined flow over a circular cylinder at different outlet boundary locations. It is clearly observed that the outlet boundary location is also playing important role in the vortex shedding process for a particular Reynolds number. For the extrapolation boundary condition on the particle distribution function at the outflow boundary to hold accurately, the boundary should be far enough downstream of the cyl-

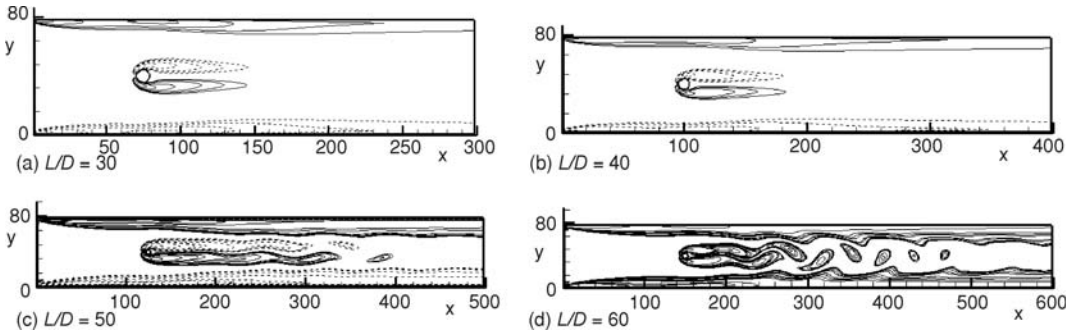


**Figure 11. Vorticity contours for flows past a circular cylinder at different outlet boundary locations for Re = 44, $l$ = 12.5D: (a) $L/D$ = 30, (b) $L/D$ = 40, (c) $L/D$ = 50, and (d) $L/D$ = 60**

inder. In our present study, simulation results reveal the fact that $L/D$ = 50 onwards periodic solutions are obtained for Re = 44.

### *Different cylinder locations*

To study the effect of different cylinder locations Re = 44 is chosen in the present work. As usual a blockage ratio of $B$ = 8 and $L/D$ = 50 are considered. All the cases studied so far take $l$ = 12.5D. In the present case, $l$ = 5.0D, 8.5D, 12.5D, 16.0D and 25.0D are considered. Figure 12 shows the instantaneous vorticity contours for confined flow over a circular cylinder for various cylinder locations. It is seen that only for the cylinder location of 12.5D and beyond the vortex shedding appears. Also differences in the size and strength of the vortices are observed as the cylinder location changes. This can be attributed to the fact that at a different cylinder locations the wall boundary layer produces different effect. Also as l increases, the exit boundary may come too near for the prescribed outflow boundary condition to hold accurately.

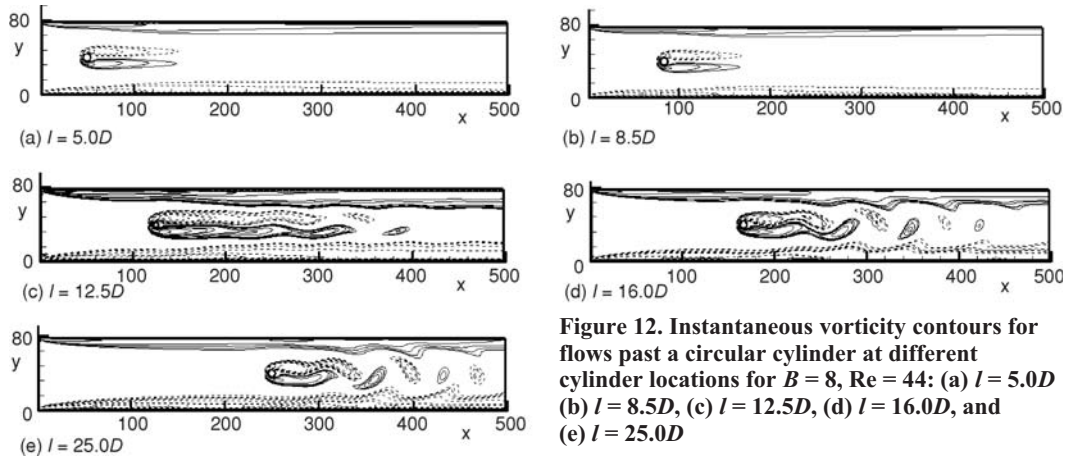


**Figure 12. Instantaneous vorticity contours for flows past a circular cylinder at different cylinder locations for $B$ = 8, Re = 44: (a) $l$ = 5.0$D$ (b) $l$ = 8.5$D$, (c) $l$ = 12.5$D$, (d) $l$ = 16.0$D$, and (e) $l$ = 25.0$D$**

## Conclusions

In this paper, LBM computation is carried out for the flow past a circular cylinder confined in a channel. Three different aspects of the problem are studied. First, for a fixed blockage

ratio computations are carried out to study the effect of Reynolds number on the flow pattern. At lower Reynolds numbers the flow is steady and a pair of stationary vortices symmetric about the channel centreline develops and remains attached to the rear side of the cylinder. As the Reynolds number increases the vortices grow in size and finally at a certain Reynolds number, the symmetry breaks and periodicity of flow sets in downstream of the cylinder. Using a plot of amplitudes of fluctuation in the x- and y-component of velocities at a downstream point, the critical Reynolds number at which unsteadiness sets in is found to be between 43 and 44, a result substantiated by experiments. Plots of u and v along the channel centerline downstream of the cylinder is also given to show that the oscillations are small at the outflow boundary where extrapolation seems appropriate to be used to determine the boundary particle distribution function. Periodic variations of the lift and drag coefficients at two Reynolds number are plotted and explanations are given for their typical behaviour. Then the effect of blockage ratio, defined in this work as the ratio of the channel width to the cylinder diameter, on the flow characteristics is studied. It is seen that lower blockage ratio tends to inhibit unsteadiness. The effect of the outlet boundary location is also studied and expectedly it is seen that keeping the boundary at a large distance downstream tends to favourably influence the accuracy of the computations. Overall it is seen that the lattice Boltzmann method can be used very effectively to produce accurate results and capture all the flow features that conventional continuum-based methods like finite difference ($F_D$) and finite volume ($F_V$) methods are capable of capturing.

## References

[1] Patel, V. A., Karman Vortex Street behind a Circular Cylinder by the Series Truncation Method, *Journal of Computational Physics, 28* (1978), 1, pp. 14-42
[2] Tritton, D. J., Experiments on the Flow Past a Circular Cylinder at Low Reynolds Numbers, *Journal of Fluid Mechanics, 6* (1959), 4, pp. 547-555
[3] Kalita, J. C., Ray, R. K., A Transformation-Free HOC Scheme for Incompressible Viscous Flows Past an Impulsively Started Circular Cylinder, *Journal of Computational Physics, 228* (2009), 14, pp. 5207-5236
[4] Fornberg, B., A Numerical Study of Steady Viscous Flow Past a Circular Cylinder, *Journal of Fluid Mechanics, 98* (1980), 4, pp. 819-855
[5] Braza, M., *et al.*, Numerical Study and Physical Analysis of the Pressure and Velocity Fields in the Near Wake of a Circular Cylinder, *Journal of Fluid Mechanics, 165* (1986), Apr., pp. 79-89
[6] Franke, R., *et al.*, Numerical Calculation of Laminar Vortex Shedding Flow Past Cylinders, *Journal of wind Engineering and Industrial Aerodynamics, 35* (1990), 1-3, pp. 237-257
[7] Calhoun, D., A Cartesian Grid Method for Solving the Two-Dimensional Streamfunction-Vorticity Equations in Irregular Regions, *Journal of Computational Physics, 176* (2002), 2, pp. 231-275
[8] Sahin, M., Owens, R. G., A Numerical Investigation of Wall Effects up to High Blockage Ratios on Two-Dimensional Flow Past a Confined Circular Cylinder, *Physics of Fluids, 16* (2004), 5, pp. 5-20
[9] Zovatto, L., Pedrizzetti, G., Flow about a Circular Cylinder between Parallel Walls, *Journal of Fluid Mechanics, 440* (2001), Aug., pp. 1-25
[10] Anagnostopoulos, P., Iliadis, G., Numerical Study of the Blockage Effects on Viscous Flow Past a Circular Cylinder, *International Journal for Numerical Methods in Fluids, 22* (1996), 11, pp. 1061-1074
[11] Singha, S., Sinhamahapatra, K. P., Flow Past a Circular Cylinder between Parallel Walls at Low Reynolds Numbers, *Journal of Ocean Engineering, 37* (2010), 8-9, pp. 757-769
[12] Perumal, D. A., Dass, A. K., Mulitplicity of Steady Solutions in Two-Dimensional Lid-Driven Cavity Flows by the Lattice Boltzmann Method, *Computers & Mathematics with Applications, 61* (2011), 12, pp. 3711-3721
[13] Perumal, D. A., Dass, A. K., Simulation of Incompressible Flows in Two-Sided Lid-Driven Square Cavities, Part II-LBM, *CFD Letters, 2* (2010), 1, pp. 25-38
[14] Yu, D., *et al*., Viscous Flow Computations with the Method of Lattice Boltzmann Equation, *Progress in Aerospace Sciences, 39* (2003), 5, pp. 329-367

[15] Hou, S., *et al.*, Simulation of Cavity Flow by the Lattice Boltzmann Method, *Journal of Computational Physics, 118* (1995), 2, pp. 329-347
[16] Bouzidi, M., *et al*., Momentum Transfer of a Lattice Boltzmann Fluid with Boundaries, *Physics of Fluids, 13* (2001), 11, pp. 3452-3459
[17] Islam, S. U., Zhou, C. Y., Numerical Simulation of Flow around a Row of Cylinders Using the Lattice Boltzmann Method, *Information Technology Journal, 8* (2009), 4, pp. 513-520
[18] Shu, C., *et al*., Taylor Series Expansion- and Least Square-Based Lattice Boltzmann Method: An Efficient Approach for Simulation of Incompressible Viscous Flows, *Progress in Computational Fluid Dynamics, 5* (2005), 1/2, pp. 27-36
[19] Ganaoui, M. E., Semma, E. A., A Lattice Boltzmann Coupled to Finite Volumes Method for Solving Phase Change Problems, *Thermal Science, 13* (2009), 2, pp. 205-216
[20] Nemati, H., *et al*., Multi-Relaxation-Time Lattice Boltzmann Model for Uniform Shear Flow over a Rotating Circular Cylinder, *Thermal Science, 15* (2011), 3, pp. 859-878
[21] Guo, Z., *et al.*, An Extrapolation Method for Boundary Conditions in Lattice Boltzmann Method, *Physics of Fluids, 14* (2002), 6, pp. 2007-2010
[22] Coutanceau, M., Bouard, R., Experimental Determination of the Main Features of the Viscous Flow in the Wake of a Circular Cylinder in Uniform Translation. Part 1: Steady Flow, *Journal of Fluid Mechanics, 79* (1977), 2, pp. 231-256
[23] De, A. K., Dalal, A., Numerical Simulation of Unconfined Flow Past a Triangular Cylinder, *International Journal for Numerical Methods in Fluids, 52* (2006), 7, pp. 801-821
[24] Sharma, V., Dhiman, A. K., Heat Transfer from a Rotating Circular Cylinder in the Steady Regime: Effects of Prandtl Number, *Thermal Science*, *16* (2012), 1, pp. 79-91
[25] Maiti, D. K., Dependence of Flow Characteristics of Rectangular Cylinders Near a Wall on the Incident Velocity, *Acta Mechanica, 222* (2011), 3, pp. 273-286

Paper submitted: September 18, 2011
Paper revised: May 9, 2012
Paper accepted: May 9, 2012